Cruz-Roldán, F., Martins, W.A., Diniz, Paulo S.R. & Moonen, M. 2019, "Achievable data rate of DCT-based multicarrier modulation systems", IEEE Transactions on Wireless Communications, vol. 18, no. 3, pp. 1739-1749

Available at http://dx.doi.org/10.1109/TWC.2019.2896073

Achievable Data Rate of DCT-based Multicarrier Modulation Systems

Fernando Cruz–Roldán, *Senior Member, IEEE,* Wallace A. Martins, *Member, IEEE*, Paulo S. R. Diniz, *Fellow, IEEE*, Marc Moonen, *Fellow, IEEE*

***Abstract*—This paper aims at studying the achievable data rate of discrete cosine transform (DCT)-based multicarrier modulation (MCM) systems. To this end, a general formulation is presented for the full transmission/reception process of data in Type−II even DCT and Type−IV even DCT-based systems. The paper focuses on the use of symmetric extension (SE) and zero padding (ZP) as redundancy methods. Furthermore, three cases related to the channel order and the length of the redundancy are studied. In the first case, the channel order is less than or equal to the length of the redundancy. In the second and third cases, the channel order is greater than the length of the redundancy; the interference caused by the channel impulse response is calculated, and theoretical expressions for their powers are derived. These expressions allow studying the achievable data rate of DCT-based MCM systems, besides enabling the comparison with the conventional MCM based on the discrete Fourier Transform.**

***Index Terms*—Multicarrier modulation (MCM), single carrier modulation (SCM), orthogonal frequency-division multiplexing (OFDM), discrete multi-tone modulation (DMT), cyclic prefix (CP), symmetric extension (SE), zero padding (ZP), discrete Fourier transform (DFT), discrete cosine transform (DCT).**

I. Introduction

IN MULTICARRIER MODULATION (MCM) systems, the frequency selective communication channel is partitioned into a set of flat fading channels, whose effects can be corrected by simply using a one-tap per subcarrier equalizer. Orthogonal frequency-division multiplexing (OFDM) and discrete multitone modulation (DMT) are examples of channel partitioning methods widely employed in wireless and wireline communication systems [1]–[4].

MCM can be implemented in several ways, but due to various advantages, such as its simplicity or effectiveness against frequency selective fading, the most popular form is based on the discrete Fourier transform (DFT). However, several authors have also proposed the use of the discrete cosine transform (DCT) [5]–[10], and in recent years this has received increasing attention in several areas, such as optical communications [11]–[15]. The DCT brings alternative capabilities and benefits derived from its energy-compaction properties, which lead to less intercarrier interference, and offers robustness against carrier frequency offset. Furthermore, DCT-based MCM (DCT-MCM) requires only half the subcarrier spacing of OFDM, thus allowing to double the number of subcarriers within the same bandwidth. DCT-MCM systems are also able to perform a good channel partitioning when redundant samples, such as in a symmetric extension (SE) [8], [16] or zero-padding (ZP) [9], [17], are included in each transmitted data vector. However, the most challenging problem in DCT-MCM is that the channel impulse response (CIR) must be symmetric. One solution to this problem is to enforce the symmetry condition of the CIR by means of a front-end prefilter at the receiver [8]. To design this prefilter, practical techniques have been proposed [8], [18].

An attractive feature of MCM systems is the possibility of using adaptive loading algorithms to improve system performance with a significant increase in the data rate per subcarrier [3]. The basic idea is to vary the data rate and power assigned to each subcarrier relative to the corresponding channel gain. This requires knowledge of the power of the intersymbol and intercarrier interference (ISI and ICI) to obtain the signal-to-interference-plus-noise ratio (SINR) and the achievable data rate. For a DFT-based MCM (DFT-MCM) system with insufficient redundant samples, different SINR models are derived in [19]–[27]. The interference calculation and the achievable data rate of a windowed OFDM are provided in [28], [29].

In this paper, we aim to determine the power of the ISI and ICI when Type−II even DCT (DCT2e) and Type−IV even DCT (DCT4e) are used for MCM. A general matrix formulation is presented for the full transmission and reception process. We consider the use of SE and ZP as redundancy methods. In our study, we also consider three different cases related to the channel order and the length of the redundancy. In the first case, the channel order is less than or equal to the length of the redundancy. In this case, the channel equalization can be carried out in the transform domain by means of a one-tap per subcarrier equalizer. The second and third cases are when the channel order is greater than the length of the redundancy. In these cases, both time-domain and transform-domain equalizations are needed to correct the

This work was supported by the Spanish Ministry of Economy and Competitiveness through Research Grant TEC2015-64835-C3-1-R, by the Spanish Ministry of Education, Culture and Sports through Research Grants PRX14/00147 and PRX17/0080, and by the Coordenação de Aperfeiçoamento de Pessoal de Nível Superior Brasil (CAPES) Finance Code 23038.009440/2012-42.

F. Cruz-Roldán is with the Department of Teoría de la Señal y Comunicaciones, Escuela Politécnica Superior de la Universidad de Alcalá, 28871 Alcalá de Henares (Madrid), SPAIN (e-mail: fernando.cruz@uah.es).

W. A. Martins and P. S. R. Diniz are with Programa of Electrical Engineering and Department of Electronics and Computer Engineering, COPPE/Poli, Universidade Federal do Rio de Janeiro, 21941-972 Rio de Janeiro-RJ, Brazil (e-mails: diniz@smt.ufrj.br; wallace.martins@smt.ufrj.br)

M. Moonen is with the Department of Electrical Engineering (ESAT), Stadius Center for Dynamical Systems, Signal Processing and Data Analytics, KU Leuven, 3001 Leuven, BELGIUM (e-mail: marc.moonen@esat.kuleuven.be).

January 25, 2019

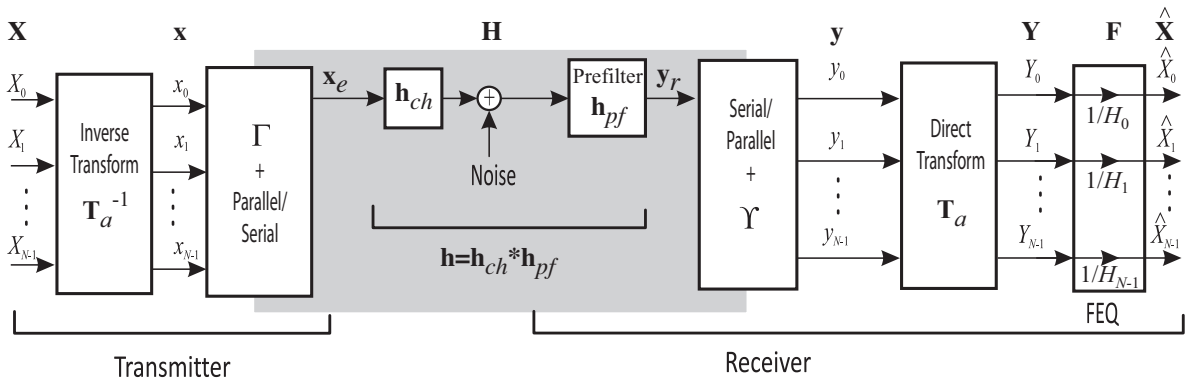

Fig. 1. General block diagram of a multicarrier transceiver over a channel with additive noise.

channel effects. We derive the expression of the SINR, which allows obtaining the achievable data rate. To the best of our knowledge, the above study for DCT-MCM systems still remains open.

This paper is organized as follows. Section II presents the MCM system model considering DCT-MCM as well as DFT-MCM as a reference system. Three types of interference caused by the CIR are calculated in Section III, using a unified formulation with SE and ZP. In Section IV, theoretical expressions for the interference powers, the SINR, and the achievable data rate are derived. In Section V, simulation results are provided to compare the achievable data rate for both DCT-MCM and DFT-MCM, and lastly, concluding remarks are made in Section VI.

The notation used in this paper is as follows. Bold-face letters indicate vectors (lower case) and matrices (upper case). $\mathbf{A}^T$ represents the transpose of $\mathbf{A}$. $\mathbf{I}_N$ denotes the $N \times N$ identity matrix. The subscript is omitted whenever the size is clear from the context. $\mathbf{J}$ stands for the counter-identity matrix, and $\mathbf{0}$ denotes a matrix of zeros.

II. MCM System Model

Fig. 1 shows the general block diagram representing the multicarrier transceiver. Let us consider the transmitted data vector in the transform domain:

$$\mathbf{X} = \left[\begin{array}{cccc} X_0 & X_1 & \cdots & X_{N-1} \end{array} \right]^T, \tag{1}$$

where N is the number of subcarriers. The time-domain data vector $\mathbf{x}$ is

$$\mathbf{x} = \mathbf{T}_a^{-1} \cdot \mathbf{X} = \left[\begin{array}{cccc} x_0 & x_1 & \cdots & x_{N-1} \end{array} \right]^T, \tag{2}$$

where $\mathbf{T}_a^{-1}$ is an N-point inverse transform. In DFT-MCM, $\mathbf{T}_a^{-1}$ is an inverse DFT ($\mathbf{W}^{-1}$) matrix with elements

$$\left[\mathbf{W}^{-1}\right]_{k,n} = \frac{1}{N} e^{j\frac{2\pi}{N}kn}.$$

In DCT-MCM, $\mathbf{T}_a^{-1}$ can be either an inverse DCT2e matrix ($\mathbf{C}_{2e}^{-1}$):

$$\left[\mathbf{C}_{2e}^{-1}\right]_{k,n} = \frac{\varphi_{2e,n}}{N} \cos\left(\frac{\pi n(2k+1)}{2N} \right),$$

with

$$\varphi_{2e,n} = \left\{ \begin{array}{ll} \frac{1}{2}, & n = 0, N-1, \\ 1, & n = 1, \ldots, N-2, \end{array} \right.$$

or an inverse DCT4e matrix ($\mathbf{C}_{4e}^{-1}$):

$$\left[\mathbf{C}_{4e}^{-1}\right]_{k,n} = \frac{1}{N} \cos\left(\frac{\pi(2n+1)(2k+1)}{4N} \right),$$

for $0 \leq k, n \leq N-1$ [30]. Then, matrix $\mathbf{\Gamma}$ introduces redundant samples into each time-domain data vector

$$\mathbf{x}_e^T = \mathbf{\Gamma} \cdot \mathbf{x} = \mathbf{\Gamma} \cdot \mathbf{T}_\mathbf{a}^{-\mathbf{1}} \cdot \mathbf{X}.$$

In DFT-MCM, the μ-length redundancy is usually either a cyclic prefix (CP) included as a left extension (LE):

$$\mathbf{x}_e^T = \mathbf{\Gamma} \cdot \mathbf{x} = \left[\begin{array}{c} \mathbf{x}_{\mu \times 1}^{LE} \\ \mathbf{x}_{N \times 1} \end{array} \right]_{(N+\mu)\times 1}, \tag{3}$$

or a ZP that can be included as a right extension (RE):

$$\mathbf{x}_e^T = \mathbf{\Gamma} \cdot \mathbf{x} = \left[\begin{array}{c} \mathbf{x}_{N \times 1} \\ \mathbf{x}_{\mu \times 1}^{RE} \end{array} \right]_{(N+\mu)\times 1}. \tag{4}$$

In DCT-MCM, the 2μ-length redundancy is basically a prefix or LE, and a suffix or RE:

$$\mathbf{x}_e^T = \mathbf{\Gamma} \cdot \mathbf{x} = \left[\begin{array}{c} \mathbf{x}_{\mu \times 1}^{LE} \\ \mathbf{x}_{N \times 1} \\ \mathbf{x}_{\mu \times 1}^{RE} \end{array} \right]_{(N+2\mu)\times 1}. \tag{5}$$

Next, the received data vector can be specified as

$$\mathbf{y}_r^T = \mathbf{H} \cdot \mathbf{x}_e^T + \mathbf{z},$$

where $\mathbf{H}$ is a (square) Toeplitz matrix formed from $\mathbf{h} = \mathbf{h}_{ch} * \mathbf{h}_{pf}$, where $\mathbf{h}_{ch}$ is the CIR, $\mathbf{h}_{pf}$ represents the impulse response of a front-end prefilter, and $\mathbf{z}$ is a column vector related to the additive noise-plus-interference. In DCT-MCM, the channel must be symmetric [8], [16]. Some channels satisfy this condition, such as chromatic dispersion in single-mode fibers [11], [13], but in most cases, a prefilter is needed to enforce this symmetry condition. For long channels, the prefilter $\mathbf{h}_{pf}$ is required for both DFT-MCM and DCT-MCM to shorten the channel. In what follows, the length of the CIR is assumed to be finite.

TABLE I
DEFINITION OF THE MATRICES USED IN THE MULTICARRIER TRANSCEIVER SYSTEMS OF FIG. 1 ($\alpha = 1$ FOR DCT2e AND $\alpha = -1$ FOR DCT4e).

Transceiver	$\mathbf{T}_a$	$\mathbf{\Gamma}$	$\mathbf{\Upsilon}$
SE DCT-MCM	$\mathbf{C}_{4e}$ or $\mathbf{C}_{2e}$	$\begin{bmatrix} \mathbf{J}_{\mu\times\mu} & \mathbf{0}_{\mu\times(N-\mu)} \\ & \mathbf{I}_N \\ \mathbf{0}_{\mu\times(N-\mu)} & \alpha\mathbf{J}_{\mu\times\mu} \end{bmatrix}$	$\begin{bmatrix} \mathbf{0}_{N\times\mu} & \mathbf{I}_N & \mathbf{0}_{N\times\mu} \end{bmatrix}$
ZP DCT-MCM	$\mathbf{C}_{4e}$ or $\mathbf{C}_{2e}$	$\begin{bmatrix} \mathbf{0}_{\mu\times N} \\ \mathbf{I}_N \\ \mathbf{0}_{\mu\times N} \end{bmatrix}$	$\begin{bmatrix} \mathbf{J}_\mu & \mathbf{I}_\mu & \mathbf{0} & \mathbf{0} & \mathbf{0} \\ \mathbf{0} & \mathbf{0} & \mathbf{I}_{N-2\mu} & \mathbf{0} & \mathbf{0} \\ \mathbf{0} & \mathbf{0} & \mathbf{0} & \mathbf{I}_\mu & \alpha\mathbf{J}_\mu \end{bmatrix}$
CP DFT-MCM	$\mathbf{W}$	$\begin{bmatrix} \mathbf{0}_{\mu\times(N-\mu)} & \mathbf{I}_{\mu\times\mu} \\ & \mathbf{I}_N \end{bmatrix}$	$\begin{bmatrix} \mathbf{0}_{N\times\mu} & \mathbf{I}_N \end{bmatrix}$
ZP DFT-MCM	$\mathbf{W}$	$\begin{bmatrix} \mathbf{I}_N \\ \mathbf{0}_{\mu\times N} \end{bmatrix}$	$\begin{bmatrix} \mathbf{I}_N & \mathbf{I}_\mu \\ & \mathbf{0}_{(N-\mu)\times\mu} \end{bmatrix}$

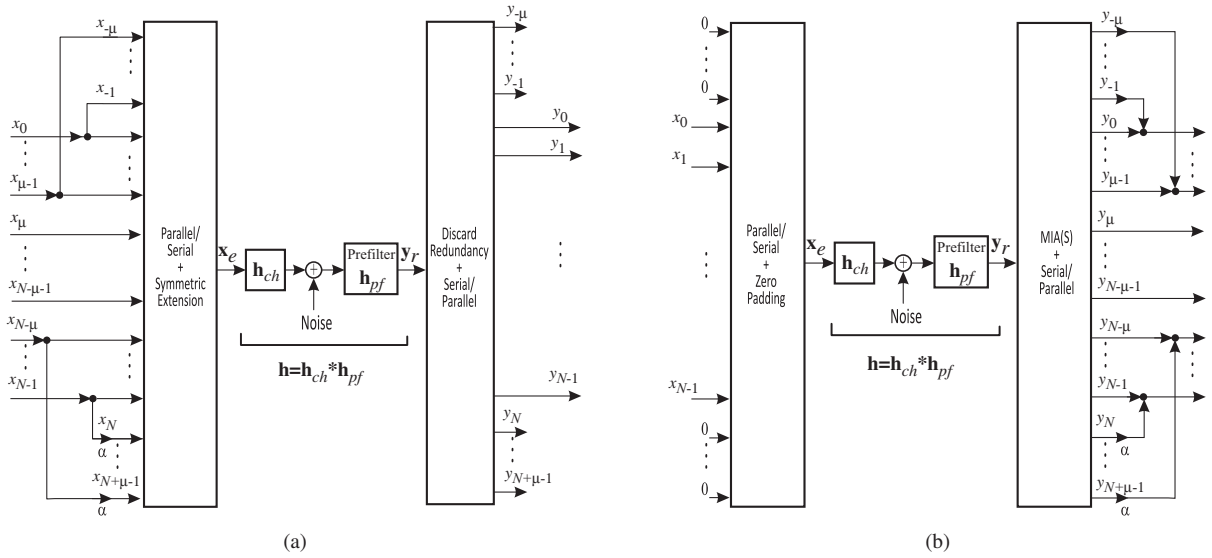

Fig. 2. Implementation of $\mathbf{\Gamma}$, $\mathbf{\Upsilon}$ and the Parallel-to-Serial (P/S) and the Serial-to-Parallel (S/P) blocks, for DCT-MCM with (a) SE and (b) ZP.

.

Next, matrix $\mathbf{\Upsilon}$ removes some samples of the received data vector: $\mathbf{y} = \mathbf{\Upsilon} \cdot \mathbf{y}_r^T$. Notice that the aim of $\mathbf{\Gamma}$ and $\mathbf{\Upsilon}$ is to turn $\mathbf{H}$ into a diagonalizable channel matrix:

$$\mathbf{H}_{eq} = \mathbf{\Upsilon} \cdot \mathbf{H} \cdot \mathbf{\Gamma} = \mathbf{T}_a^{-1} \cdot \mathbf{D} \cdot \mathbf{T}_a,$$

where $\mathbf{D}$ is a diagonal matrix with elements H_k, $0 \leq k \leq (N-1)$. Table I includes the full definition of the matrices $\mathbf{\Gamma}$ and $\mathbf{\Upsilon}$ used in Fig. 1. These matrices $\mathbf{\Upsilon}$ and $\mathbf{\Gamma}$ are implemented for DCT-MCM as follows. If an SE is used as redundancy, the parallel-to-serial and the serial-to-parallel blocks are configured as in Fig. 2(a). On the other hand, an overlapping applied to the received signal is required when ZP is used as redundancy, as depicted in Fig. 2(b). This overlapping is a process of mirror and add and subtract (MIAS [17]), or mirror and add (MIA [31]), and it depends on the type of DCT used in the multicarrier transceiver.

As shown in Fig. 1, after matrix $\mathbf{\Upsilon}$, an N-point transform $\mathbf{T}_a$ is performed, resulting in the transform domain received data vector

$$\mathbf{Y} = \mathbf{T}_a \cdot \mathbf{y} = \mathbf{T}_a \cdot \mathbf{\Upsilon} \cdot \mathbf{y}_r^T,$$

where $\mathbf{T}_a$ is a DFT matrix ($\mathbf{W}$):

$$[\mathbf{W}]_{k,n} = e^{-j\frac{2\pi}{N}kn},$$

or a DCT2e ($\mathbf{C}_{2e}$):

$$[\mathbf{C}_{2e}]_{k,n} = 2\cos\left(\frac{\pi(2n+1)k}{2N}\right), \tag{6}$$

or a DCT4e ($\mathbf{C}_{4e}$):

$$[\mathbf{C}_{4e}]_{k,n} = 2\cos\left(\frac{\pi(2n+1)(2k+1)}{4N}\right). \tag{7}$$

Finally, the vector $\mathbf{Y}$ is equalized in the transform domain by means of one-tap per subcarrier equalizer with complex coefficient $1/H_k$, and decoded to reconstruct the transmitted data.

III. ANALYSIS OF INTERFERENCE

This section analyzes the interference for DCT-MCM. Important parameters to be considered are the order ν of the CIR, the length 2μ of the redundancy, and the order 2ν of the composite model comprised of the cascade of CIR and front-end prefilter. The number of data vectors affecting the reception of a single data vector in DCT-MCM is $2M+1$, where

$$M = \left\lceil \frac{2\nu}{N+2\mu} \right\rceil, \tag{8}$$

and $\lceil\cdot\rceil$ stands for the ceiling function. In the following subsection, we address the case $\nu \leq \mu$. Without loss of generality, we analyze the above case considering the most critical instance, i.e., $\nu = \mu$. Next, we provide insight into the case with $\nu > \mu$, where different kinds of interference are analyzed.

A. Case 1: $\nu \leq \mu$

The useful samples of the received data vector can be expressed as

$$\mathbf{y} = \begin{bmatrix} y_0 \\ \vdots \\ y_{N-1} \end{bmatrix} = \boldsymbol{\Upsilon} \cdot \mathbf{H} \cdot \boldsymbol{\Gamma} \begin{bmatrix} x_0 \\ \vdots \\ x_{N-1} \end{bmatrix} + \begin{bmatrix} z_0 \\ \vdots \\ z_{N-1} \end{bmatrix}. \quad (9)$$

For DCT-MCM, a prefilter $\mathbf{h}_{pf}$ is needed, which enforces the symmetry condition[1]. Defining

$$\mathbf{h} = \mathbf{h}_{ch} * \mathbf{h}_{pf} = \begin{bmatrix} h_0 & \cdots & h_\nu & \cdots & h_{2\nu} \end{bmatrix}, \quad (10)$$

the Toeplitz matrix $\mathbf{H}$ is an $(N+2\mu) \times (N+2\mu)$ matrix, defined as

$$\mathbf{H} = \begin{bmatrix} h_\nu & h_{\nu-1} & \cdots & h_0 & 0 & \cdots & \cdots & 0 \\ h_{\nu+1} & h_\nu & h_{\nu-1} & \cdots & h_0 & 0 & \ddots & \vdots \\ \vdots & & & & & & & \\ h_{2\nu} & & & & & & & \\ 0 & h_{2\nu} & \cdots & h_\nu & \cdots & h_0 & 0 & \vdots \\ \vdots & & \ddots & & & & \ddots & 0 \\ & \ddots & \ddots & & & & & h_0 \\ & & & & & & & \vdots \\ \vdots & & 0 & h_{2\nu} & & \cdots & h_\nu & h_{\nu-1} \\ 0 & \cdots & & 0 & h_{2\nu} & \cdots & h_{\nu+1} & h_\nu \end{bmatrix}. \quad (11)$$

In this case, a synchronization delay of $\Delta = \nu$ is assumed for a proper DCT-MCM operation. In what follows, we assume a symmetric channel $\mathbf{h}$, i.e., $h_i = h_{2\nu-i}$, $0 \leq i \leq 2\nu$. With the above assumption, $\mathbf{H}$ is given by

$$\mathbf{H} = \begin{bmatrix} h_\nu & h_{\nu+1} & \cdots & h_{2\nu} & 0 & \cdots & \cdots & 0 \\ h_{\nu+1} & h_\nu & h_{\nu+1} & \cdots & h_{2\nu} & 0 & \ddots & \vdots \\ \vdots & & & & & & & \\ h_{2\nu} & & & & & & & \\ 0 & h_{2\nu} & \cdots & h_\nu & \cdots & h_{2\nu} & 0 & \vdots \\ \vdots & & \ddots & & & & \ddots & 0 \\ & \ddots & \ddots & & & & & h_{2\nu} \\ & & & & & & & \vdots \\ \vdots & & 0 & h_{2\nu} & & \cdots & h_\nu & h_{\nu+1} \\ 0 & \cdots & & 0 & h_{2\nu} & \cdots & h_{\nu+1} & h_\nu \end{bmatrix}. \quad (12)$$

Let us consider now the matrices of Table I. The product $\boldsymbol{\Upsilon} \cdot \mathbf{H} \cdot \boldsymbol{\Gamma}$ is given as

$$\mathbf{H}_{eq} = \boldsymbol{\Upsilon} \cdot \mathbf{H} \cdot \boldsymbol{\Gamma} = (\mathbf{H}_H + \mathbf{H}_T) = \left(\begin{bmatrix} h_{\nu+1} & \cdots & h_{2\nu} & 0 & \cdots & 0 \\ \vdots & \iddots & \iddots & & \iddots & \vdots \\ h_{2\nu} & \iddots & & \iddots & & 0 \\ 0 & & \iddots & & \iddots & \alpha h_{2\nu} \\ \vdots & \iddots & & \iddots & \iddots & \vdots \\ 0 & \cdots & 0 & \alpha h_{2\nu} & \cdots & \alpha h_{\nu+1} \end{bmatrix} + \begin{bmatrix} h_\nu & \cdots & h_{2\nu} & 0 & \cdots & 0 \\ \vdots & \ddots & \ddots & \ddots & \ddots & \vdots \\ h_{2\nu} & \ddots & \ddots & \ddots & \ddots & 0 \\ 0 & \ddots & \ddots & \ddots & \ddots & h_{2\nu} \\ \vdots & \ddots & \ddots & \ddots & \ddots & \vdots \\ 0 & \cdots & 0 & h_{2\nu} & \cdots & h_\nu \end{bmatrix} \right). \quad (13)$$

As can be seen, $\mathbf{H}_{eq}$ is expressed as the sum of a Hankel matrix $\mathbf{H}_H$ and a Toeplitz matrix $\mathbf{H}_T$, and thus it can be diagonalized by DCTs [30]:

$$\mathbf{H}_{eq} = \mathbf{C}^{-1} \cdot \mathbf{D} \cdot \mathbf{C} = \mathbf{C}^{-1} \cdot \begin{bmatrix} H_0 & 0 & \cdots & 0 \\ 0 & H_1 & \cdots & \vdots \\ \vdots & \ddots & \ddots & 0 \\ 0 & \cdots & 0 & H_{N-1} \end{bmatrix} \cdot \mathbf{C}, \quad (14)$$

where either $\mathbf{C} = \mathbf{C}_{2e}$ or $\mathbf{C} = \mathbf{C}_{4e}$. Furthermore, as demonstrated in [16], [17], the diagonal elements H_k of (14)

[1]There are several techniques available to design this prefilter [8], [18]. Here, the prefilter is assumed of finite length $\nu + 1$.

can be obtained as follows:

$$\begin{bmatrix} H_0 \\ \vdots \\ H_{N-1} \end{bmatrix} = \begin{bmatrix} \frac{1}{\xi_0} & 0 & \cdots & 0 \\ 0 & \frac{1}{\xi_1} & \cdots & 0 \\ \vdots & \ddots & \ddots & \vdots \\ 0 & \cdots & 0 & \frac{1}{\xi_{N-1}} \end{bmatrix} \times \left(\mathbf{C} \cdot \begin{bmatrix} h_\nu + h_{\nu+1} \\ \vdots \\ h_{2\nu-1} + h_{2\nu} \\ h_{2\nu} \\ 0 \\ \vdots \\ 0 \end{bmatrix} \right), \quad (15)$$

where:

i) For DCT2e: $\mathbf{C} = \mathbf{C}_{2e}$ and $\xi_k = 2\cos\frac{k\pi}{2N}$,

ii) For DCT4e: $\mathbf{C} = \mathbf{C}_{4e}$ and $\xi_k = 2\cos\frac{(2k+1)\pi}{4N}$,

for $0 \leq k \leq N-1$.

The received data vector in the transform domain is then given as

$$\mathbf{Y} = \mathbf{T}_a \cdot \begin{bmatrix} y_0 \\ \vdots \\ y_{N-1} \end{bmatrix} = \mathbf{T}_a \cdot \mathbf{H}_{eq} \cdot \mathbf{T}_a^{-1} \cdot \begin{bmatrix} X_0 \\ \vdots \\ X_{N-1} \end{bmatrix} + \mathbf{T}_a \cdot \begin{bmatrix} z_0 \\ \vdots \\ z_{N-1} \end{bmatrix}, \quad (16)$$

or equivalently

$$\begin{bmatrix} Y_0 \\ \vdots \\ Y_{N-1} \end{bmatrix} = \left(\begin{bmatrix} H_0 & 0 & \cdots & 0 \\ 0 & H_1 & \ddots & \vdots \\ \vdots & \ddots & \ddots & 0 \\ 0 & \cdots & 0 & H_{N-1} \end{bmatrix} \times \begin{bmatrix} X_0 \\ \vdots \\ X_{N-1} \end{bmatrix} \right) + \begin{bmatrix} Z_0 \\ \vdots \\ Z_{N-1} \end{bmatrix}. \quad (17)$$

Then, the transmitted data vector can be reconstructed as:

$$\hat{\mathbf{X}} = \mathbf{D}^{-1} \cdot \mathbf{Y}, \quad (18)$$

where $\mathbf{D}^{-1}$ is an $N \times N$ diagonal matrix with elements $[\mathbf{D}]_{k,k}^{-1} = 1/H_k$.

B. Case 2: $\mu < \nu \leq \frac{N}{2} + \mu$

In this subsection, we derive an expression for the received signal when the order of the channel is greater than the length of the redundancy and $M = 1$. In this case, the received data vector at time l is affected only by the data vector transmitted at time l, the previous data vector transmitted at time $l-1$, and the next data vector transmitted at time $l+1$. This often occurs in many practical communication systems and it is equivalent to using a sufficiently large number of useful subcarriers N to guarantee that $N \geq 2(\nu - \mu)$.

Let the time-domain data vector $\mathbf{x}[l]$ be defined as

$$\mathbf{x}[l] = \begin{bmatrix} x_0[l] \\ \vdots \\ x_{N-1}[l] \end{bmatrix}, \quad (19)$$

and $\mathbf{x}[l \pm m]$, with $m \in \{-1, 1\}$, be similarly defined. The received data vector $\mathbf{y}[l]$ can then be specified as

$$\begin{aligned} \mathbf{y}[l] &= \begin{bmatrix} y_0[l] \\ \vdots \\ y_{N-1}[l] \end{bmatrix} \\ &= \boldsymbol{\Upsilon} \cdot \mathbf{H}_{(-1)} \cdot \boldsymbol{\Gamma} \cdot \mathbf{x}[l-1] + \boldsymbol{\Upsilon} \cdot \mathbf{H}_1 \cdot \boldsymbol{\Gamma} \cdot \mathbf{x}[l+1] \\ &+ \boldsymbol{\Upsilon} \cdot \mathbf{H}_0 \cdot \boldsymbol{\Gamma} \cdot \mathbf{x}[l] \\ &+ \boldsymbol{\Upsilon} \cdot \mathbf{H}_{pf,0} \cdot \mathbf{q}[l] + \boldsymbol{\Upsilon} \cdot \mathbf{H}_{pf,1} \cdot \mathbf{q}[l+1], \end{aligned} \quad (20)$$

where $\mathbf{q}[l+m]$ is a noise vector,

$$\mathbf{H}_{(-1)} = \begin{bmatrix} \mathbf{0}_{(N+2\mu)\times(N+2\mu-\nu)} & \mathbf{H}^a_{(N+2\mu)\times\nu} \end{bmatrix},$$

$$\mathbf{H}_1 = \begin{bmatrix} \mathbf{H}^f_{(N+2\mu)\times\nu} & \mathbf{0}_{(N+2\mu)\times(N+2\mu-\nu)} \end{bmatrix},$$

with

$$\mathbf{H}^a_{(N+2\mu)\times\nu} = \begin{bmatrix} h_{2\nu} & \cdots & h_{\nu+1} \\ 0 & \ddots & \vdots \\ & \ddots & h_{2\nu} \\ \vdots & & 0 \\ & & \vdots \\ 0 & \cdots & 0 \end{bmatrix},$$

$$\mathbf{H}^f_{(N+2\mu)\times\nu} = \begin{bmatrix} 0 & \cdots & 0 \\ \vdots & & \\ 0 & & \vdots \\ h_0 & \ddots & \\ \vdots & \ddots & 0 \\ h_{\nu-1} & \cdots & h_0 \end{bmatrix},$$

and the Toeplitz matrix $\mathbf{H}_0$ is defined as in (11). Notice that due to the symmetry condition of $\mathbf{h}$, we have that $\mathbf{H}_0$ is given by (12) and $\mathbf{H}_1 = \mathbf{H}^T_{(-1)}$. Finally, $\mathbf{H}_{pf,0}$ is an $(N+2\mu) \times N$ Toeplitz matrix with first row

$$\begin{bmatrix} h_{pf,\nu} & h_{pf,\nu-1} & \cdots & h_{pf,0} & 0 & \cdots & 0 \end{bmatrix}$$

and first column $[h_{pf,\nu} \quad 0 \quad \cdots \quad 0]^T$. As for $\mathbf{H}_{pf,1}$, it shares the same structure of $\mathbf{H}_1$, but again with the coefficients of $\mathbf{h}_{pf}$ and replacing matrix $\mathbf{0}_{(N+2\mu)\times(N+2\mu-\nu)}$ with matrix $\mathbf{0}_{(N+2\mu)\times(N-\nu)}$. In the definitions of $\mathbf{H}_{pf,0}$ and $\mathbf{H}_{pf,1}$ we assumed $N \geq \nu + 1$ to simplify notation, without loss of generality for the case $M = 1$.

The received data vector $\mathbf{Y}[l]$ in the transform domain is then given as

$$\begin{aligned}\mathbf{Y}[l] &= \begin{bmatrix} Y_0[l] \\ \vdots \\ Y_{N-1}[l] \end{bmatrix} \\ &= \sum_{m=-1}^{1} \mathbf{T}_a \cdot \boldsymbol{\Upsilon} \cdot \mathbf{H}_m \cdot \boldsymbol{\Gamma} \cdot \mathbf{x}[l+m] \\ &\quad + \sum_{m=0}^{1} \mathbf{T}_a \cdot \boldsymbol{\Upsilon} \cdot \mathbf{H}_{pf,m} \cdot \mathbf{q}[l+m] \end{aligned} \quad (21)$$

The transmitted data vector can be reconstructed as

$$\begin{aligned}\hat{\mathbf{X}}[l] &= \begin{bmatrix} \hat{X}_0[l] \\ \vdots \\ \hat{X}_{N-1}[l] \end{bmatrix} = \mathbf{D}^{-1} \cdot \mathbf{Y}[l] \\ &= \mathbf{D}^{-1} \cdot \underbrace{\mathbf{T}_a \cdot \boldsymbol{\Upsilon} \cdot \mathbf{H}_{(-1)} \cdot \boldsymbol{\Gamma} \cdot \mathbf{T}_a^{-1}}_{\mathbf{A}_1^{\mathrm{ISI,ICI_2}}} \cdot \mathbf{X}[l-1] \\ &\quad + \mathbf{D}^{-1} \cdot \underbrace{\mathbf{T}_a \cdot \boldsymbol{\Upsilon} \cdot \mathbf{H}_0 \cdot \boldsymbol{\Gamma} \cdot \mathbf{T}_a^{-1}}_{\mathbf{B}^{\mathrm{des,ICI_1}}} \cdot \mathbf{X}[l] \\ &\quad + \mathbf{D}^{-1} \cdot \underbrace{\mathbf{T}_a \cdot \boldsymbol{\Upsilon} \cdot \mathbf{H}_1 \cdot \boldsymbol{\Gamma} \cdot \mathbf{T}_a^{-1}}_{\mathbf{F}_1^{\mathrm{ISI,ICI_2}}} \cdot \mathbf{X}[l+1] \\ &\quad + \mathbf{D}^{-1} \cdot \underbrace{\mathbf{T}_a \cdot \boldsymbol{\Upsilon} \cdot \mathbf{H}_{pf,0}}_{\mathbf{G}_0^{\mathrm{noise}}} \cdot \mathbf{q}[l] \\ &\quad + \mathbf{D}^{-1} \cdot \underbrace{\mathbf{T}_a \cdot \boldsymbol{\Upsilon} \cdot \mathbf{H}_{pf,1}}_{\mathbf{G}_1^{\mathrm{noise}}} \cdot \mathbf{q}[l+1]. \end{aligned} \quad (22)$$

The desirable signal of (22) is

$$\hat{\mathbf{X}}_{\mathrm{des}}[l] = \mathbf{D}^{-1} \cdot \mathbf{B}^{\mathrm{des}} \cdot \mathbf{X}[l], \quad (23)$$

where $\mathbf{B}^{\mathrm{des}}$ is an $N \times N$ diagonal matrix with elements

$$\left[\mathbf{B}^{\mathrm{des}}\right]_{i,i} = \left[\mathbf{B}^{\mathrm{des,ICI_1}}\right]_{i,i}.$$

In the absence of noise, the difference between (22) and (23) defines the ICI and ISI (see Fig. 3), and it is the consequence of an insufficient length of the redundancy. In the previous case $\nu \leq \mu$, one has $M = 1$, but it is interesting to notice that matrices $\boldsymbol{\Upsilon}$ and $\boldsymbol{\Gamma}$ are able to completely eliminate the interference induced by the data vectors transmitted at $l-1$ and $l+1$. Nonetheless, when $\nu > \mu \geq 1$, the interference cannot be completely eliminated using either matrices $\boldsymbol{\Upsilon}$ or $\boldsymbol{\Gamma}$, eventually degrading the system performance. Furthermore, the products $\boldsymbol{\Upsilon} \cdot \mathbf{H}_m \cdot \boldsymbol{\Gamma}$, cannot be expressed as $N \times N$ Hankel-plus-Toeplitz matrices, and therefore they cannot be diagonalized using DCTs.

C. Case 3: $\nu > \frac{N}{2} + \mu$

In this subsection, a general expression for the reconstructed data vector when $M > 1$ is derived. Let $\mathbf{x}[l \pm m]$, $m \in \{0, 1, \cdots, M\}$, be defined as in (19). In this case, the received data vector $\mathbf{y}[l]$ is given by

$$\mathbf{y}[l] = \sum_{m=-M}^{M} \boldsymbol{\Upsilon} \cdot \mathbf{H}_m \cdot \boldsymbol{\Gamma} \cdot \mathbf{x}[l+m] + \sum_{m=0}^{M} \boldsymbol{\Upsilon} \cdot \mathbf{H}_{pf,m} \cdot \mathbf{q}[l+m]. \quad (24)$$

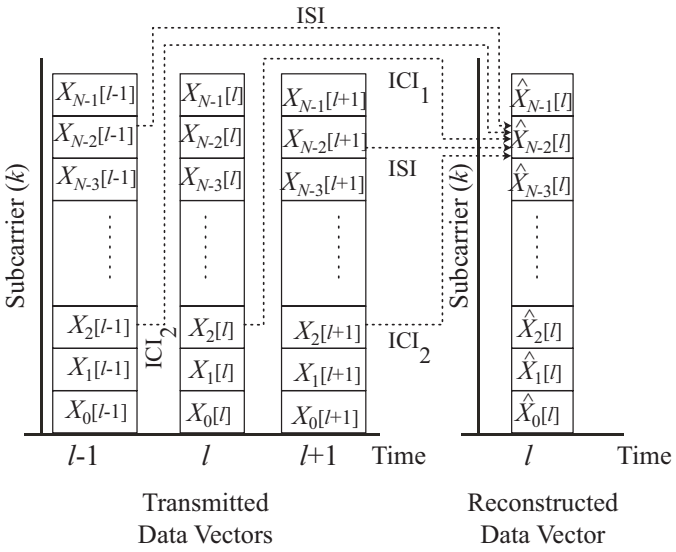

Fig. 3. Types of interference.

In the above,

$$[\mathbf{H}_m]_{b,c} = \begin{cases} h_{\kappa_1}, & \kappa_1 \in \{0, 1, \cdots, 2\nu\}, \\ 0, & \text{otherwise}, \end{cases} \quad (25)$$

$$[\mathbf{H}_{pf,m}]_{b,d} = \begin{cases} h_{pf,\kappa_2}, & \kappa_2 \in \{0, 1, \cdots, \nu\}, \\ 0, & \text{otherwise}, \end{cases} \quad (26)$$

where $0 \leq b, c \leq N + 2\mu - 1$, $\kappa_1 = \nu - m(N + 2\mu) + b - c$, $0 \leq d \leq N - 1$, and $\kappa_2 = \nu - m(N + 2\mu) + b - d$. It is worth pointing out that $\mathbf{h}_{pf}$ is not symmetric and that again, the products $\boldsymbol{\Upsilon} \cdot \mathbf{H}_m \cdot \boldsymbol{\Gamma}$, for $m \in \{-M, -M+1, \cdots, M-1, M\}$, cannot be expressed as $N \times N$ Hankel-plus-Toeplitz matrices. In this case, the reconstructed data vector can be expressed as follows:

$$\begin{aligned}\hat{\mathbf{X}}[l] &= \sum_{m=1}^{M} \mathbf{D}^{-1} \cdot \underbrace{\mathbf{T}_a \cdot \boldsymbol{\Upsilon} \cdot \mathbf{H}_{(-m)} \cdot \boldsymbol{\Gamma} \cdot \mathbf{T}_a^{-1}}_{\mathbf{A}_m^{\mathrm{ISI,ICI_2}}} \cdot \mathbf{X}[l-m] \\ &\quad + \mathbf{D}^{-1} \cdot \underbrace{\mathbf{T}_a \cdot \boldsymbol{\Upsilon} \cdot \mathbf{H}_0 \cdot \boldsymbol{\Gamma} \cdot \mathbf{T}_a^{-1}}_{\mathbf{B}^{\mathrm{des,ICI_1}}} \cdot \mathbf{X}[l] \\ &\quad + \sum_{m=1}^{M} \mathbf{D}^{-1} \cdot \underbrace{\mathbf{T}_a \cdot \boldsymbol{\Upsilon} \cdot \mathbf{H}_m \cdot \boldsymbol{\Gamma} \cdot \mathbf{T}_a^{-1}}_{\mathbf{F}_m^{\mathrm{ISI,ICI_2}}} \cdot \mathbf{X}[l+m] \\ &\quad + \sum_{m=0}^{M} \mathbf{D}^{-1} \cdot \underbrace{\mathbf{T}_a \cdot \boldsymbol{\Upsilon} \cdot \mathbf{H}_{pf,m}}_{\mathbf{G}_m^{\mathrm{noise}}} \cdot \mathbf{q}[l+m]. \end{aligned} \quad (27)$$

The desirable part of (27) is also given by (23), and the difference between (27) and (23) defines the ISI, ICI, and the noise for $M > 1$. Based on [23], [32], the interference is classified into three types:

- ISI: This is the interference from the data vector transmitted at time $l \pm m$, with $m \in \{1, 2, \cdots, M\}$, in the considered data vector transmitted at time l on the same subcarrier. All diagonal elements $a_{i,i}$ and $f_{i,i}$ in matrices $\mathbf{A}_m = \mathbf{A}_m^{\mathrm{ISI,ICI_2}}$ and $\mathbf{F}_m = \mathbf{F}_m^{\mathrm{ISI,ICI_2}}$, respectively, contribute to this interference.

- Type 1 ICI (ICI_1): This is the interference among different subcarriers belonging to the considered data vector transmitted at time l. It appears as a consequence of the elements $b_{i,j}^{\text{ICI}_1}$ in matrix $\mathbf{B}^{\text{ICI}_1} = \mathbf{B}^{\text{des,ICI}_1} - \mathbf{B}^{\text{des}}$.
- Type 2 ICI (ICI_2): This is the interference among different subcarriers of the data vector transmitted at time $l \pm m$, with $m \in \{1, 2, \cdots, M\}$, in the considered data vector transmitted at time l. The elements $a_{i,j}$ and $f_{i,j}$, $i \neq j$, in matrices $\mathbf{A}_m = \mathbf{A}_m^{\text{ISI,ICI}_2}$ and $\mathbf{F}_m = \mathbf{F}_m^{\text{ISI,ICI}_2}$, respectively, contribute to this interference.

Finally, the contribution of noise $\mathbf{q}[l+m]$ to the reconstructed data vector $\hat{\mathbf{X}}[l]$ depends on matrix $\mathbf{G}_m^{\text{noise}}$.

IV. Achievable Data Rate

Once the ICI, ISI, and the noise have been determined, we can derive analytical expressions for the achievable data rate. We assume constellations of infinite granularity so that each subcarrier can carry a fractional and unbounded number of bits. We also assume that the data vector components X_k and noise vector components q_k are zero-mean wide-sense stationary (WSS) uncorrelated processes. Moreover, X_k and q_k are assumed independent and identically distributed (i.i.d.) for all k, with variances σ_X^2 and σ_n^2, respectively.

The desirable received data vector component $Y_{\text{des},k}$ can be written as

$$Y_{\text{des},k} = \underbrace{\mathbf{T}_{a,k} \cdot \boldsymbol{\Upsilon} \cdot \mathbf{H}_0^{\text{des}} \cdot \boldsymbol{\Gamma} \cdot \mathbf{T}_a^{-1}}_{\mathbf{B}_k^{\text{des}}} \cdot \mathbf{X}[l], \tag{28}$$

where $\mathbf{T}_{a,k}$ represents the kth row of $\mathbf{T}_a$. Thus, the useful signal power (before the transform-domain equalization) at subcarrier k is given by

$$\begin{aligned} P_{\text{signal}}(k) &= E\left\{Y_{\text{des},k} \cdot Y_{\text{des},k}^H\right\} \\ &= E\left\{\mathbf{B}_k^{\text{des}} \cdot \mathbf{X}[l] \cdot \mathbf{X}^H[l] \cdot \left(\mathbf{B}_k^{\text{des}}\right)^H\right\} \\ &= \mathbf{B}_k^{\text{des}} \cdot E\left\{\mathbf{X}[l] \cdot \mathbf{X}^H[l]\right\} \cdot \left(\mathbf{B}_k^{\text{des}}\right)^H. \\ &= \sigma_X^2 \cdot \mathbf{B}_k^{\text{des}} \cdot \left(\mathbf{B}_k^{\text{des}}\right)^H, \end{aligned} \tag{29}$$

where $E\{\cdot\}$ is the expected value. On the other hand, the noise data vector is given by

$$Y_{\text{noise},k} = \sum_{m=0}^{M} \mathbf{G}_{m,k}^{\text{noise}} \cdot \mathbf{q}[l+m], \tag{30}$$

where $\mathbf{G}_{m,k}^{\text{noise}}$ is defined as $\mathbf{G}_m^{\text{noise}}$ by replacing $\mathbf{T}_a$ by $\mathbf{T}_{a,k}$. Then, the noise power is given by

$$\begin{aligned} P_{\text{noise}}(k) &= \sum_{m=0}^{M} E\left\{\mathbf{G}_{m,k}^{\text{noise}} \cdot \mathbf{q}[l+m] \cdot \mathbf{q}^H[l+m] \cdot \left(\mathbf{G}_{m,k}^{\text{noise}}\right)^H\right\} \\ &= \sigma_n^2 \cdot \sum_{m=0}^{M} \mathbf{G}_{m,k}^{\text{noise}} \cdot \left(\mathbf{G}_{m,k}^{\text{noise}}\right)^H. \end{aligned} \tag{31}$$

Finally, the interference component is defined by the following difference

$$\begin{aligned} Y_{\text{int},k} &= Y_k - Y_{\text{des},k} - Y_{\text{noise},k} \\ &= \sum_{m=1}^{M} \mathbf{A}_{m,k} \cdot \mathbf{X}[l-m] \\ &\quad + \left(\mathbf{B}_k^{\text{des,ICI}_1} - \mathbf{B}_k^{\text{des}}\right) \cdot \mathbf{X}[l] \\ &\quad + \sum_{m=1}^{M} \mathbf{F}_{m,k} \cdot \mathbf{X}[l+m] \\ &= \mathbf{B}_k^{\text{ICI}_1} \cdot \mathbf{X}[l] \\ &\quad + \sum_{m=1}^{M} \left(\mathbf{A}_{m,k} \cdot \mathbf{X}[l-m] + \mathbf{F}_{m,k} \cdot \mathbf{X}[l+m]\right), \end{aligned} \tag{32}$$

where $\mathbf{A}_{m,k}$, $\mathbf{B}_k^{\text{ICI}_1}$, and $\mathbf{F}_{m,k}$ are defined as $\mathbf{A}_m$, $\mathbf{B}^{\text{ICI}_1}$, and $\mathbf{F}_m$, respectively, by replacing $\mathbf{T}_a$ by $\mathbf{T}_{a,k}$. As a result, the ISI and ICI power can be expressed as

$$\begin{aligned} &P_{\text{ISI,ICI}}(k) = E\left\{Y_{\text{int},k} \cdot Y_{\text{int},k}^H\right\} \\ = \; & E\left\{\mathbf{B}_k^{\text{ICI}_1} \cdot \mathbf{X}[l] \cdot \mathbf{X}^H[l] \cdot \left(\mathbf{B}_k^{\text{ICI}_1}\right)^H\right\} \\ & + \sum_{m=1}^{M} E\left\{\mathbf{A}_{m,k} \cdot \mathbf{X}[l-m] \cdot \mathbf{X}^H[l-m] \cdot \left(\mathbf{A}_{m,k}\right)^H\right\} \\ & + \sum_{m=1}^{M} E\left\{\mathbf{F}_{m,k} \cdot \mathbf{X}[l+m] \cdot \mathbf{X}^H[l+m] \cdot \left(\mathbf{F}_{m,k}\right)^H\right\} \\ = \; & \sigma_X^2 \cdot \mathbf{B}_k^{\text{ICI}_1} \cdot \left(\mathbf{B}_k^{\text{ICI}_1}\right)^H \\ & + \sigma_X^2 \cdot \sum_{m=1}^{M} \left(\mathbf{A}_{m,k} \cdot \left(\mathbf{A}_{m,k}\right)^H + \mathbf{F}_{m,k} \cdot \left(\mathbf{F}_{m,k}\right)^H\right). \end{aligned} \tag{33}$$

With the expressions (29), (31), and (33), the SINR for subcarrier k is given by (34).

When M-PSK modulation is used, the achievable data rate for subcarrier k is given by [33]

$$C(k) = \frac{1}{2} \log_2 \left(\frac{\text{SINR}(k)}{\gamma^*}\right), \tag{35}$$

where γ^* is the modified SINR gap defined for a target symbol error rate (SER) as

$$\gamma^* = \left(\frac{Q^{-1}(\text{SER}/2)}{\sqrt{2}\pi}\right)^2.$$

For $\gamma^* = 1$, $C(k)$ is the capacity of the kth subchannel. The achievable data rate is finally obtained as

$$R = f_s \sum_{k=0}^{N-1} \frac{N}{N_0} \cdot C(k), \tag{36}$$

where

i) For DFT-MCM: $N_0 = N + \mu$ and $f_s = 1/T_s$,
ii) For DCT-MCM: $N_0 = N + 2\mu$ and $f_s = 1/(2T_s)$.

$$\begin{aligned}\mathrm{SINR}\,(k) &= \frac{P_{\mathrm{signal}}\,(k)}{P_{\mathrm{ISI,ICI}}\,(k)+P_{\mathrm{noise}}\,(k)} \\ &= \frac{\sigma_X^2\cdot\mathbf{B}_k^{\mathrm{des}}\cdot\left(\mathbf{B}_k^{\mathrm{des}}\right)^H}{\sigma_X^2\cdot\left(\mathbf{B}_k^{\mathrm{ICI}_1}\cdot\left(\mathbf{B}_k^{\mathrm{ICI}_1}\right)^H+\sum_{m=1}^{M}\left(\mathbf{A}_{m,k}\cdot\left(\mathbf{A}_{m,k}\right)^H+\mathbf{F}_{m,k}\cdot\left(\mathbf{F}_{m,k}\right)^H\right)\right)+\sigma_n^2\cdot\sum_{m=0}^{M}\mathbf{G}_{m,k}^{\mathrm{noise}}\cdot\left(\mathbf{G}_{m,k}^{\mathrm{noise}}\right)^H}\end{aligned} \tag{34}$$

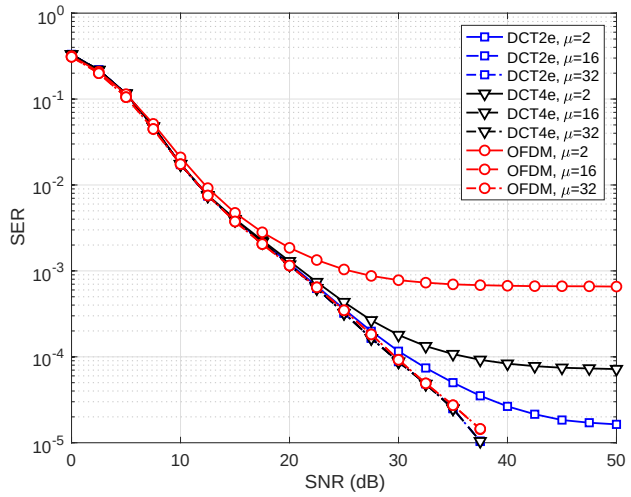

(a) PED200

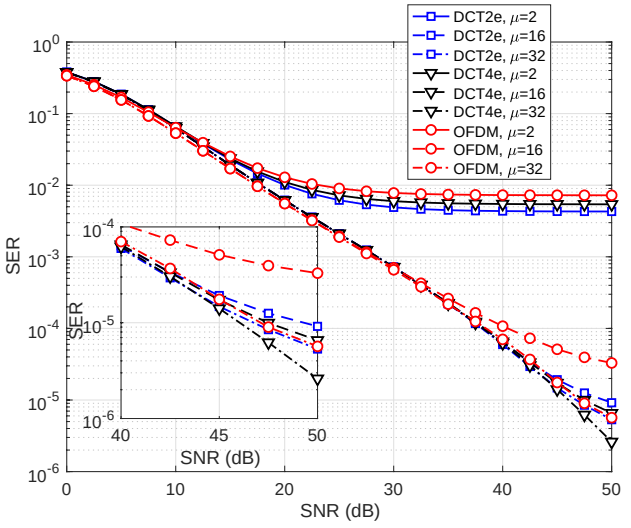

(b) VEH200

Fig. 4. SER for several channels and multicarrier transceivers using different lengths for the redundancy.

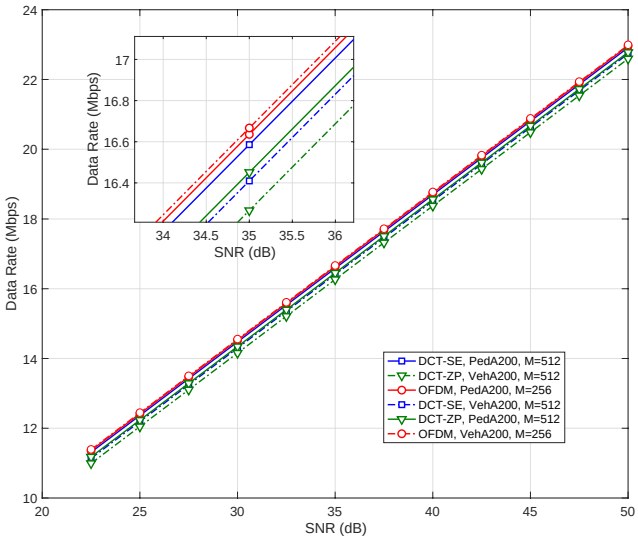

Fig. 5. Achievable data rate versus SNR for different multicarrier transceivers and channels.

V. Simulations

In this section, simulation results are presented to evaluate the achievable data rate of DCT-MCM (DCT2e-MCM and DCT4e-MCM) obtained with (36) and using the SINR given by (34). The results are compared with those for DFT-MCM (OFDM), but in the latter, we use the SINR derived in [34]. In our simulations, we assume BPSK modulation and systems with 512 (DCT-MCM) and 256 (DFT-MCM) active subcarriers. Perfect synchronization and channel estimation are also assumed at the receiver. The results for several kinds of redundancies are shown, namely CP for DFT-MCM, and SE and ZP for the DCT-MCM. Similar simulations have been carried out including ZP as redundancy for DFT-MCM, and the results have been practically indistinguishable. For this reason, these are not included. The number of redundant samples varies for each simulation with the aim of studying its effects on the achievable data rate. Although the theoretical analysis is general, we shall consider only the most common case where $M = 1$ in these simulations, for the sake of conciseness. The noise is modeled as additive white Gaussian noise (AWGN). We assume that the channel remains unchanged within the same simulation. Two sets of 250 wireless fading channels each, according to the ITU Pedestrian A and Vehicular A channels [35], [36], are used as multipath channels. They have been generated with Matlab's `stdchan` using the channel models `itur3GPAx` and `itur3GVAx` with a carrier frequency $f_c = 2$ GHz and two different sets of parameters: (a) 4 km per hour as pedestrian velocity, $T_s = 200$ ns and length $L = \nu + 1 = 11$; (b) 100 km per hour as mobile speed, $T_s = 200$ ns and length $L = \nu + 1 = 21$. These channels are referred to as PED200 and VEH200, respectively. The frequency spacings are 5.5804 kHz (DCT-MCM) and 11.16071492 kHz (DFT-MCM). The front-end prefilter for DCT-MCM is implemented as the time-reversed (matched) filter to the estimated channel. For DFT-MCM, no prefilter is employed.

TABLE II
VALUES FOR THE SNR, THE TARGET SER AND γ^*.

SNR (dB)	SER	γ^*
5	10^{-1}	0.1371
25	10^{-3}	0.5485
45	10^{-4}	0.7668

We first investigate the BER performance of DCT-MCM compared to DFT-MCM with different lengths of th redundancies. This study completes those previously reporte in [8], [9], [16], [17]. In addition, it is also useful for data rat comparisons, because it allows to determine the SNR value for which a target SER is achieved, and therefore, the γ values to be used in the following simulation. Fig. 4 depicts th BER obtained over the two different channels. For the PED20 channel, we first observe a performance degradation due to a insufficient number of redundant samples (CP=2, SE=2). I this case, DCT2e-MCM provides the best performance. Fo DFT-MCM, the SER curve reaches an error floor at a lowe SNR. For the other simulations, the results of DFT-MCM an DCT-MCM are almost indistinguishable. This also holds fo the VEH200 channel, in which the results are quite similar fo the three different transceivers. In these cases, there is not on transceiver that significantly improves the BER performanc compared to the other transceivers.

Next, simulation results are presented to investigate th data rate performance for a length of the redundancy fixe to $\mu = 32$. This is sufficient to perform a correct channe partitioning for both the PED200 and the VEH200. Based on the results of Fig. 4, the SNR must be at least 22.5 dB to get an achievable target SER less than or equal to 10^{-3}, which corresponds to $\gamma^* = 0.5485$. Fig. 5 shows the data rate as a function of the SNR. Given that the results have been practically indistinguishable for DCT2e and DCT4e, only one curve to represent DCT-MCM is included. It is seen that DFT-MCM slightly outperforms DCT-MCM (0.1 or 0.2 Mbps) for all the SNR values evaluated. In addition, DCT-MCM with SE exhibits better performance than their ZP counterpart.

In our last set of simulations, we study the influence of the number of redundant samples on the achievable data rate. Considering the results of the first simulation, we employ the SNR values, the target SER, and γ^* given in Table II. The results for the PED200 and VEH200 are shown in Figs. 6(a) and 6(b), respectively. In both cases, the results have been practically indistinguishable for DCT2e and DCT4e. Furthermore, for all SNR values evaluated, DCT-MCM with SE and ZP outperform DFT-MCM operating with insufficient redundant samples. This improvement is more significant for a smaller number of redundant samples for PED200. It is seen that DCT-MCM with ZP closely matches the performance of DCT-MCM with SE. Note, however, that DFT-MCM performs slightly better than DCT-MCM for larger redundancy lengths; the difference in the achievable data rate is quite small, below 0.2 Mbps for PED200 and 0.5 Mbps for VEH200.

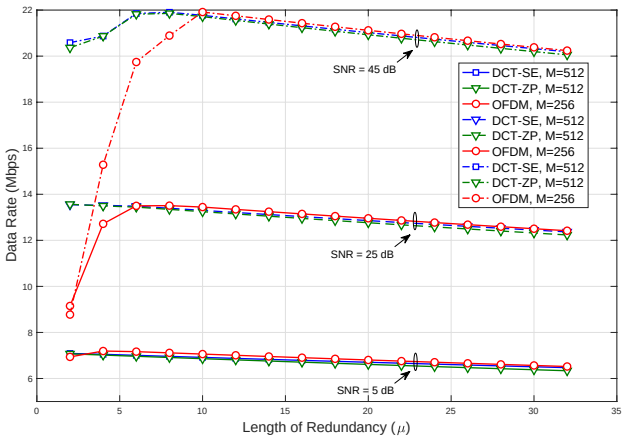

(a) PED200

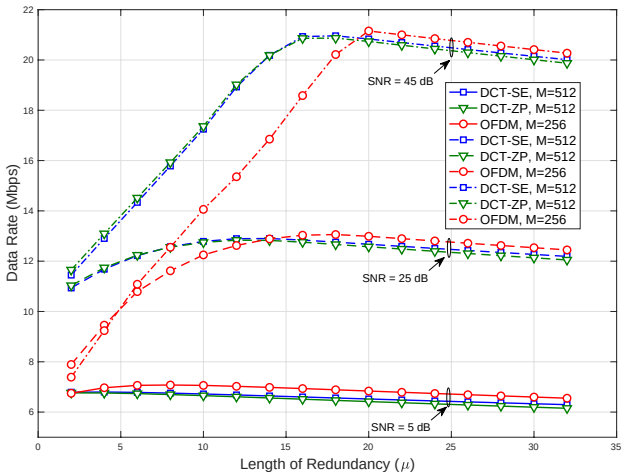

(b) VEH200

Fig. 6. Achievable data rate for different lengths for the redundancy and different SNR values.

VI. CONCLUSION

This paper has focused on the formulation of DCT-MCM for different kinds (SE and ZP) and lengths of the inserted redundancy. As is well known, the use of a redundancy for each transmitted data vector enables correcting the channel effects, provided that the length of the redundancy is at least equal to the order of the channel. Otherwise, interference occurs and successful recovery of the transmitted data is compromised. In this paper, expressions for the intersymbol and the intercarrier interference, and also for the noise have been derived. These expressions have been used to study the achievable data rate. Furthermore, computer simulations have been carried out, and several cases have been identified in which DCT-MCM is more effective than DFT-MCM in terms of data rate. In comparison to DFT-MCM, DCT-MCM provides data rate gains when an insufficient number of redundant samples is used. This advantage, along with the good behavior of DCT-MCM under carrier frequency offset reported in previous literature, makes DCT-MCM an interesting alternative to DFT-MCM.

ACKNOWLEDGEMENTS

The authors would like to thank the Associate Editor and the anonymous Reviewers for their insightful recommendations, which have significantly contributed to the improvement of this paper.

REFERENCES

[1] J. A. C. Bingham, "Multicarrier modulation for data transmission: An idea whose time has come," *IEEE Communications Magazine*, vol. 28, no. 5, pp. 5–14, May 1990.

[2] Y.-P. Lin, S.-M. Phoong, and P. P. Vaidyanathan, *Filter Bank Transceivers for OFDM and DMT systems*. Cambridge University Press, 2011.

[3] J. Cioffi, "Digital communications, chap. 4: Multichannel modulation," https://web.stanford.edu/group/cioffi/doc/book/chap4.pdf.

[4] P. S. R. Diniz, W. A. Martins, and M. V. S. Lima, *Block Transceivers: OFDM and Beyond*. Morgan & Claypool, 2012.

[5] S. Attallah and J. E. M. Nilsson, "Sequences leading to minimum peak-to-average power ratios for DCT-based multicarrier modulation," *Electronics Letters*, vol. 34, no. 15, pp. 1469–1470, 23 July 1998.

[6] J. Tan and G. L. Stüber, "Constant envelope multi-carrier modulation," in *Proceedings of the MILCOM 2002*, 7-10 Oct. 2002, pp. 607–611.

[7] G. D. Mandyam, "Sinusoidal transforms in OFDM systems," *IEEE Transactions on Broadcasting*, vol. 50, no. 2, pp. 172–184, June 2004.

[8] N. Al-Dhahir, H. Minn, and S. Satish, "Optimum DCT-based multicarrier transceivers for frequency-selective channels," *IEEE Transactions on Communications*, vol. 54, no. 5, pp. 911–921, May 2006.

[9] P. Tan and N. C. Beaulieu, "A comparison of DCT-based OFDM and DFT-based OFDM in frequency offset and fading channels," *IEEE Transactions on Communications*, vol. 54, no. 11, pp. 2113–2125, Nov. 2006.

[10] F. Gao, T. Cui, A. Nallanathan, and C. Tellambura, "Maximum likelihood based estimation of frequency and phase offset in DCT OFDM systems under non-circular transmissions: Algorithms, analysis and comparisons," *IEEE Transactions on Communications*, vol. 56, pp. 1425–1429, Sep. 2008.

[11] J. Zhao and A. Ellis, "Transmission of 4-ASK optical fast OFDM with chromatic dispersion compensation," *IEEE Photonics Technology Letters*, vol. 24, no. 1, pp. 34–36, Jan. 2012.

[12] ——, "Advantage of optical fast OFDM over OFDM in residual frequency offset compensation," *IEEE Photonics Technology Letters*, vol. 24, no. 24, pp. 2284–2287, Dec. 2012.

[13] X. Ouyang and J. Zhao, "Single-tap equalization for fast OFDM signals under generic linear channels," *IEEE Communications Letters*, vol. 18, no. 8, pp. 1319–1322, Aug. 2014.

[14] L. Zhao, J. He, Z. Zhou, R. Deng, and L. Chen, "The research of optical fast OFDM based on channel estimation algorithm," *IEEE Photonics Journal*, vol. 8, no. 3, pp. 1–5, June 2016.

[15] J. Zhou, Y. Qiao, T. Zhang, E. Sun, M. Guo, Z. Zhang, X. Tang, and F. Xu, "FOFDM based on discrete cosine transform for intensity-modulated and direct-detected systems," *Journal of Lightwave Technology*, vol. 34, no. 16, pp. 3717–3725, Aug. 2016.

[16] F. Cruz–Roldán, M. Domínguez-Jiménez, G. Sansigre–Vidal, P. Amo–López, M. Blanco–Velasco, and Á. Bravo–Santos, "On the use of discrete cosine transforms for multicarrier communications," *IEEE Transactions on Signal Processing*, vol. 11, no. 11, pp. 6085–6090, Nov. 2012.

[17] F. Cruz–Roldán, M. Domínguez-Jiménez, G. Sansigre–Vidal, J. Piñeiro–Ave, and M. Blanco–Velasco, "Single-carrier and multicarrier transceivers based on discrete cosine transform type-IV," *IEEE Transactions on Wireless Communications*, vol. 12, no. 12, pp. 6454–6463, Dec. 2013.

[18] F. Cruz–Roldán, M. Domínguez-Jiménez, G. Sansigre–Vidal, D. Luengo, and M. Moonen, "DCT-based channel estimation for single- and multicarrier communications," *Signal Processing*, vol. 128, pp. 332–339, 2016.

[19] N. Al-Dhahir and J. M. Cioffi, "Optimum finite-length equalization for multicarrier transceivers," *IEEE Transactions on Communications*, vol. 44, no. 1, pp. 56–64, Jan. 1996.

[20] ——, "A bandwidth-optimized reduced-complexity equalized multicarrier transceiver," *IEEE Transactions on Communications*, vol. 45, no. 8, pp. 948–956, Aug. 1997.

[21] D. Kim and G. L. Stuber, "Residual ISI cancellation for OFDM with applications to HDTV broadcasting," *IEEE Journal on Selected Areas in Communications*, vol. 16, no. 8, pp. 1590–1599, Oct. 1998.

[22] G. Arslan, B. L. Evans, and S. Kiaei, "Equalization for discrete multitone transceivers to maximize bit rate," *IEEE Transactions on Signal Processing*, vol. 49, no. 12, pp. 3123–3135, Dec. 2001.

[23] K. Van Acker, "Equalization and echo cancellation for DMT-based DSL modems," Ph.D. dissertation, Katholieke Universiteit Leuven, Belgium, 2001.

[24] W. Henkel, G. Tauböck, P. Ödling, P. O. Börjesson, and N. Petersson, "The cyclic prefix of OFDM/DMT - An analysis," in *Proceedings of 2002 International Zurich Seminar on Broadband Communications. Access, Transmission, Networking*, 2002, pp. 22–1–22–3.

[25] M. Milošević, L. F. C. Pessoa, B. L. Evans, and R. Baldick, "DMT bit rate maximization with optimal time domain equalizer filter bank architecture," in *Conference Record of the Thirty-Sixth Asilomar Conference on Signals, Systems and Computers*, vol. 1, Nov. 2002, pp. 377–382.

[26] T. Pham, T. Le-Ngoc, G. K. Woodward, and P. A. Martin, "Channel estimation and data detection for insufficient cyclic prefix MIMO-OFDM," *IEEE Transactions on Vehicular Technology*, vol. 66, no. 6, pp. 4756–4768, June 2017.

[27] B. Lim and Y. C. Ko, "SIR analysis of OFDM and GFDM waveforms with timing offset, CFO, and phase noise," *IEEE Transactions on Wireless Communications*, vol. 16, no. 10, pp. 6979–6990, Oct. 2017.

[28] P. Achaichia, M. L. Bot, and P. Siohan, "OFDM/OQAM: A solution to efficient increase the capacity of future PLC networks," *IEEE Transactions on Power Delivery*, vol. 26, no. 4, pp. 2443–2455, Oct. 2011.

[29] T. Nhan-Vo, K. Amis, T. Chonavel, and P. Siohan, "Achievable throughput optimization in OFDM systems in the presence of interference and its application to power line networks," *IEEE Transactions on Communications*, vol. 62, no. 5, pp. 1704–1715, May 2014.

[30] V. Sánchez, P. García, A. M. Peinado, J. C. Segura, and A. J. Rubio, "Diagonalizing properties of the discrete cosine transform," *IEEE Transactions on Signal Processing*, vol. 43, no. 11, pp. 2631–2641, Nov. 1995.

[31] M. Domínguez-Jiménez, G. Sansigre–Vidal, and F. Cruz–Roldán, "On the use of zero padding with discrete cosine transform type-ii in multicarrier communications," in *Proceedings of 22nd European Signal Processing Conference (EUSIPCO-2014)*, Lisbon (Portugal), Sep. 2014.

[32] T. Pollet, H. Steendam, and M. Moeneclaey, "Performance degradation of multi-carrier systems caused by an insufficient guard interval," in *Proceedings of CWAS'97-Intern.Workshop on Copper Wire Access Systems "Bridging the Last Copper Drop"*, Budapest, Hongarije, 27-29 Oct 1997, pp. 265–270.

[33] A. García-Armada, "SNR gap approximation for M-PSK-based bit loading," *IEEE Transactions on Wireless Communications*, vol. 5, no. 1, pp. 57–60, Jan. 2006.

[34] W. A. Martins, F. Cruz–Roldán, M. Moonen, and P. S. R. Diniz, "Intersymbol and intercarrier interference in OFDM transmissions through highly dispersive channels," arXiv:1901.08142, 2019.

[35] "Recommendation ITU-R M.1225: Guidelines for evaluation of radio transmission technologies for IMT-2000," 1997.

[36] 3rd Generation Partnership Project, 3GPP TS 25.101, *Technical Specification Group Radio Radio Access Network. User Equipment (UE) Radio Transmission and Reception (FDD) (Release 7)*, Sep. 2007.

Fernando Cruz–Roldán (M'98, SM'06) was born in Baena, Spain, in 1968. He received his Technical Telecommunication Engineer degree from the Universidad de Alcalá (UAH), Spain, in 1990, his Telecommunication Engineer degree from the Universidad Politécnica de Madrid (UPM), Spain, in 1996, and Ph. D. in Electrical Engineering from the UAH, in 2000. Dr. Cruz-Roldán received the Universidad de Alcalá Prize for the most outstanding doctoral dissertation in the engineering discipline.

He joined the Department of Ingeniería de Circuitos y Sistemas (UPM), in 1990, where from 1993 to 2003, he was an Assistant Professor. From 1998 to February 2003, he was a Visiting Lecturer at Universidad de Alcalá. In March 2003, he joined the Universidad de Alcalá, Spain, as an Associate Professor, and since November 2009, he has been a Professor with the Department of Teoría de la Señal y Comunicaciones, Universidad de Alcalá.

His teaching and research interests are in digital signal processing, filter design, and multirate systems applied to subband coding and broadband digital communications.

Wallace A. Martins (S'06, M'12) was born in Brazil in 1983. He received the Electronics Engineer degree from the Federal University of Rio de Janeiro (UFRJ) in 2007, the M.Sc. and D.Sc. degrees in Electrical Engineering also from UFRJ in 2009 and 2011, respectively. He was a Research Visitor at University of Notre Dame (USA, 2008), at Université Lille 1 (France, 2016), and at Universidad de Alcalá (Spain, 2018). From 2010 to 2013 he was an Associate Professor of the Federal Center for Technological Education Celso Suckow da Fonseca (CEFET/RJ). Since 2013 he has been with the Department of Electronics and Computer Engineering (DEL/Poli) and Electrical Engineering Program (PEE/COPPE) at UFRJ, where he is presently an Associate Professor (on leave). He is currently a Research Associate working with the Interdisciplinary Centre for Security, Reliability and Trust (SnT) at Université du Luxembourg (Luxembourg, 2019). His research interests are in the fields of digital signal processing, adaptive signal processing, graph signal processing, and digital communications, especially satellite communications, massive MIMO systems, and visible light communications. Dr. Martins received the Best Student Paper Award from EURASIP at EUSIPCO-2009, Glasgow, Scotland, and the 2011 Best Brazilian D.Sc. Dissertation Award from Capes.

Paulo S. R. Diniz (M'81, SM'92, F'00) was born in Niterói, Brazil. He received the Electronics Eng. degree (Cum Laude) from the Federal University of Rio de Janeiro (UFRJ) in 1978, the M.Sc. degree from COPPE/UFRJ in 1981, and the Ph.D. from Concordia University, Montreal, P.Q., Canada, in 1984, all in electrical engineering. His teaching and research interests are in analog and digital signal processing, adaptive signal processing, digital communications, wireless communications, multirate systems, stochastic processes, and electronic circuits.

He has published refereed papers in journals and conference papers in some of these areas, and wrote the text books *ADAPTIVE FILTERING: Algorithms and Practical Implementation*, Fourth Edition, Springer, NY, 2013, and *DIGITAL SIGNAL PROCESSING: System Analysis and Design*, Second Edition, Cambridge University Press, Cambridge, UK, 2010 (with E. A. B. da Silva and S. L. Netto), and the monograph *BLOCK TRANSCEIVERS: OFDM and Beyond*, Morgan & Claypool, New York, NY, 2012 (W. A. Martins, and M. V. S. Lima).

He is a Fellow of IEEE (2000) and EURASIP (2016). He has served as associate editor for the following Journals: IEEE Transactions on Circuits and Systems II: Analog and Digital Signal Processing from 1996 to 1999, IEEE Transactions on Signal Processing from 1999 to 2002, and the Circuits, Systems and Signal Processing Journal from 1998 to 2002. He was a distinguished lecturer of the IEEE Circuits and Systems Society for the year 2000 to 2001. In 2004 he served as distinguished lecturer of the IEEE Signal Processing Society and received the 2014 Charles Desoer Technical Achievement Award of the IEEE Circuits and Systems Society. He also holds some best-paper awards from conferences and from an IEEE journal.

Prof. P. S. R. Diniz is a member of the National Academy of Engineering (ANE), and of the Brazilian Academy of Science (ABC).

Marc Moonen (M'94, SM'06, F'07) is a Full Professor at the Electrical Engineering Department of KU Leuven, where he is heading a research team working in the area of numerical algorithms and signal processing for digital communications, wireless communications, DSL and audio signal processing. He is a Fellow of the IEEE (2007) and a Fellow of EURASIP (2018).

He received the 1994 KU Leuven Research Council Award, the 1997 Alcatel Bell (Belgium) Award (with Piet Vandaele), the 2004 Alcatel Bell (Belgium) Award (with Raphael Cendrillon), and was a 1997 Laureate of the Belgium Royal Academy of Science. He received journal best paper awards from the IEEE Transactions on Signal Processing (with Geert Leus and with Daniele Giacobello) and from Elsevier Signal Processing (with Simon Doclo).

He was chairman of the IEEE Benelux Signal Processing Chapter (1998-2002), a member of the IEEE Signal Processing Society Technical Committee on Signal Processing for Communications, and President of EURASIP (European Association for Signal Processing, 2007-2008 and 2011-2012). He has served as Editor-in-Chief for the EURASIP Journal on Applied Signal Processing (2003-2005), Area Editor for Feature Articles in IEEE Signal Processing Magazine (2012-2014), and has been a member of the editorial board of Signal Processing, IEEE Transactions on Circuits and Systems II, IEEE Signal Processing Magazine, Integration-the VLSI Journal, EURASIP Journal on Wireless Communications and Networking and EURASIP Journal on Advances in Signal Processing.